PROCEEDINGS OF SCIENCE

# Production of Heavy Flavor in ATLAS

**R. Novotný, on behalf of the ATLAS collaboration**

*Department of Physics and Astronomy, University of New Mexico, Albuquerque, NM, USA, 87131*

*E-mail:* radek.novotny@cern.ch

The ATLAS experiment at the Large Hadron collider measures various heavy flavor production processes. This paper focuses on the measurement of $W$ boson production in association with a charmed hadron in $pp$ collisions at 13 TeV as well as on the production of $\Upsilon(nS)$ mesons in $Pb+Pb$ and $pp$ collisions at 5.02 TeV. Both of these analyses are important for the understanding of the heavy flavor properties under various conditions.

*21st International Conference on B-Physics at Frontier Machines (Beauty2023)*
*3-7 July, 2023*
*Clermont-Ferrand, France*





PoS(BEAUTY2023)042

## 1. W boson production in association with a charmed hadron

In perturbative quantum chromodynamics (QCD), the production of a $W$ boson in association with a single charm quark occurs through the scattering of a gluon and a down-type quark. The dominant production process at the Large Hadron Collider (LHC) [1] is $gs \to W^- c$ and its charge conjugate. The process $gd \to W^- c (g\bar{d} \to W^+ \bar{c})$ contributes only $\sim 10\%(5\%)$ to the $W^- c (W^+ \bar{c})$ rate. The leading-order diagrams for $W^- + c$ production are shown in Figure 1.

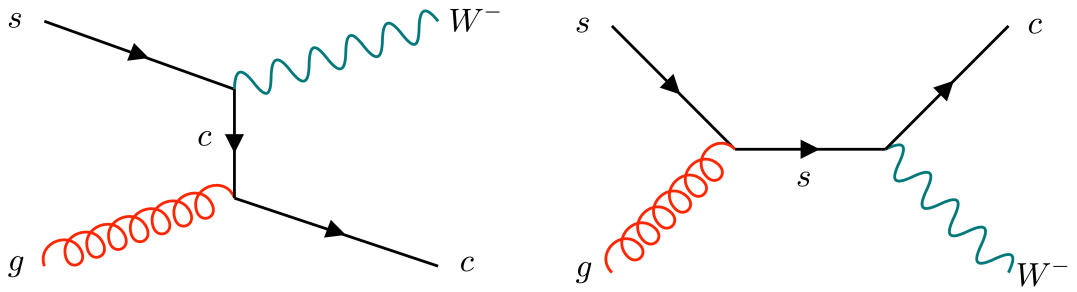


**Figure 1:** The leading-order diagrams for $W^- + c$ production. Taken from [3].

The ATLAS experiment [2] studied production of a $W$ boson in association with a single charm quark using 140 fb$^{-1}$ of $\sqrt{s} = 13$ TeV $pp$ collisions [3]. To study this type of process, the ATLAS measurement examines the $W$ boson in association with the $D^{(*)}$ meson. The analysis procedure is based on a study of events in which the $W$ boson decays to an electron or a muon ($W \to e\nu$ and $W \to \mu\nu$) and the presence of the charm quark is detected through explicit charmed hadron reconstruction. Events are required to have exactly one lepton, so events with additional leptons are rejected. To reduce multijet background, $E_{\mathrm{T}}^{miss} > 30$ GeV and $m_{\mathrm{T}}(W) > 60$ GeV is required.

Events containing c-quarks are identified by explicitly reconstructing charmed mesons in charged, hadronic decay channels. The production of charmed hadrons is studied using the decay modes $D^+ \to K^-\pi^+\pi^+$ and $D^{*+} \to D^0\pi^+ \to (K^-\pi^+)\pi^+$. In the case of multiple $D^{(*)}$ candidates, all combinations are taken into account.

The selected events are categorized according to their $b-$jet multiplicity to separate $W + D^{(*)}$ signal events from the $t\bar{t}$ background with events containing $W \to cs$ decays. Events with 0 $b-$jets are classified into the $W + D^{(*)}$ signal region (**SR**). Events with one or more $b-$tag jets comprise the Top control region (**CR**).

Monte Carlo (MC) samples are used to construct signal and background mass templates except for the multijet background. Samples produced with various MC generators are processed using a full detector simulation based on Geant4 [4] and then reconstructed using the same algorithms as the data. The hadronization rates are reweighted to the world-average values [6, 7].

For the multijet background, a data-driven approach based on the Matrix Method is used [5]. It arises from the cases when one or more constituents of a jet are misidentified as a prompt lepton. Figure 2 demonstrates the extrapolation of the multijet background from the Fake CR to the $W+D^{(*)}$ SR for the electron channel. To validate the extrapolation, the prediction is evaluated in a validation region (**VR**) with an $m_{\mathrm{T}}$ requirement of 40 GeV $< m_{\mathrm{T}} <$ 60 GeV. Figure 2 shows that the prediction

in the VR is in agreement with the data within the systematic uncertainties, indicating that the multijet background is modeled well enough.

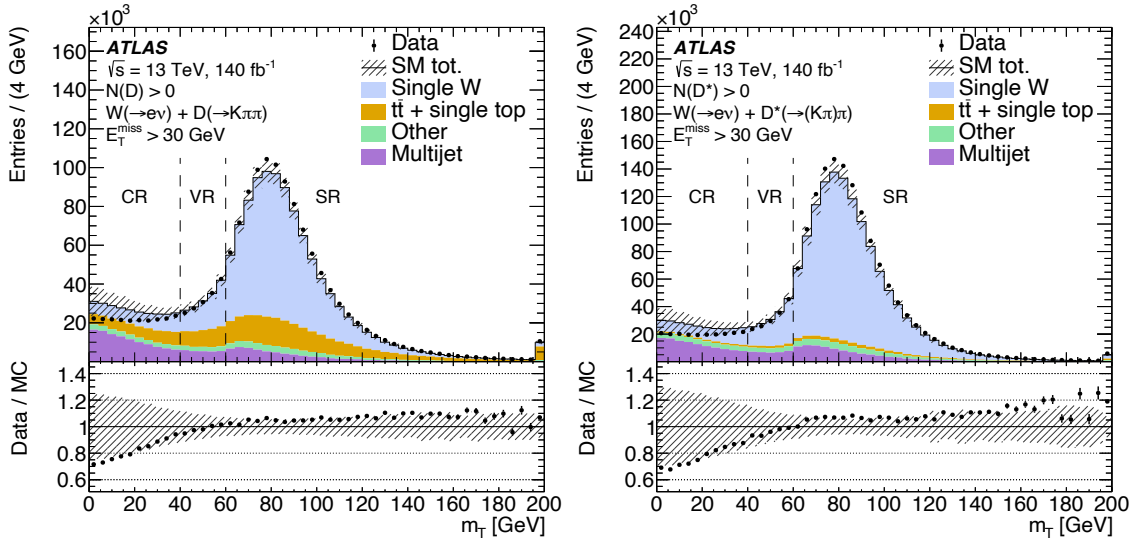


**Figure 2:** Modeling distributions of the transverse mass ($m_{\mathrm{T}}$) variable using the Matrix Method to estimate the multijet background. The distributions for $m_{\mathrm{T}}$ in the $D^{+}$ (left) and $D^{*+}$ (right) electron channel is shown. Taken from [3].

The analysis exploits the charge correlations of the $W$ boson and the charm quark to enhance the signal since the signal has $W$ and $D^{(*)}$ with opposite charge (OS), while the background is mostly the same sign (SS). The signal is extracted by measuring the difference in the number of OS and SS candidates. The signal $W + D^{(*)}$ events are extracted through a profile likelihood fit to the reconstructed secondary vertex mass distribution measuring:

- absolute fiducial cross-section: $\sigma_{\mathrm{fid}}^{OS-SS}(W^{-} + D^{(*)})$ and $\sigma_{\mathrm{fid}}^{OS-SS}(W^{+} + D^{(*)})$,
- cross-section ratio: $R_c^{\pm} = \sigma_{\mathrm{fid}}^{OS-SS}(W^{+} + D^{(*)})/\sigma_{\mathrm{fid}}^{OS-SS}(W^{-} + D^{(*)})$, and
- differential cross-sections for OS-SS $W^{-} + D^{(*)}$ and $W^{+} + D^{(*)}$.

The differential cross-section is made in 5 bins of $p_{\mathrm{T}}(D^{(*)})$ and 5 bins of $|\eta(l)|$. The example of the differential cross-section comparisons between the data and theoretical predictions obtained using different NNLO PDF sets is shown in Figure 3. Figure 4 shows the example of the measured fiducial cross-section times the single-lepton-flavor $W$ branching ratio compared with different NNLO PDF predictions for the $W^{-} + D^{+}$, and the measured fiducial cross-section ratio, $R_c^{\pm}$. The full set of results can be found in Ref. [3].

The uncertainty in the measured absolute integrated and differential fiducial cross-sections is about 5% and is dominated by systematic uncertainty. On the other hand, cross-section ratios and normalized differential cross-sections are measured with percent-level precision and have comparable contributions from systematic and statistical uncertainties. The experimental precision of these measurements is comparable to the PDF uncertainties and smaller than the total theory uncertainty.

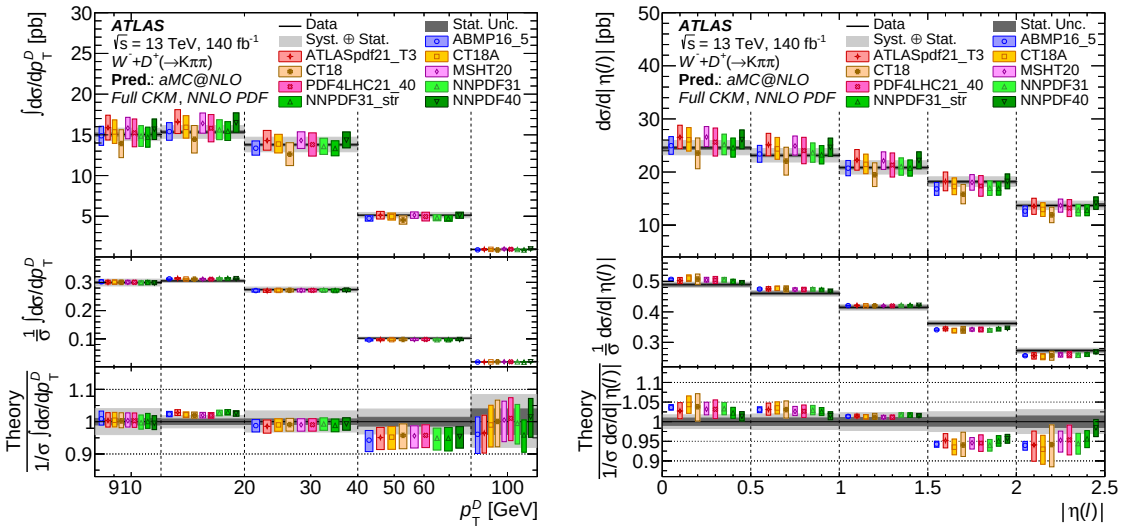


**Figure 3:** Measured differential fiducial cross-section times the single-lepton-flavor $W$ branching ratio compared with different NNLO PDF predictions in the $D^+$ channel: $W^- + D^+ p_{\mathrm{T}}(D^+)$ (left) and $W^- + D^+ |\eta(l)|$ (right). Taken from [3].

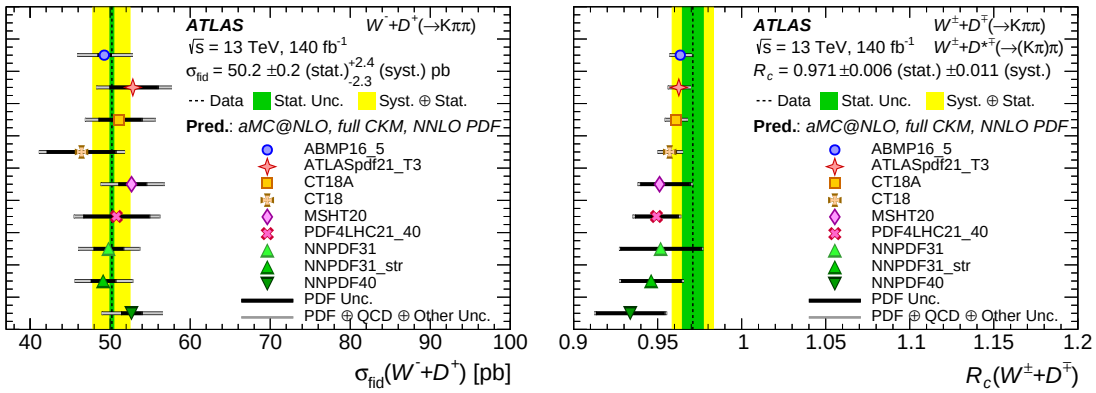


**Figure 4:** Measured fiducial cross-section times the single-lepton-flavor $W$ branching ratio compared with different NNLO PDF predictions for the $W^- + D^+$ (left) and the measured fiducial cross-section ratio, $R_c^{\pm}$ (right). Taken from [3].

## 2. Production of $\Upsilon(nS)$ mesons in $Pb+Pb$ and $pp$ collisions at 5.02 TeV

Quantum chromodynamics (QCD) predicts a phase transition at high temperatures and energy densities and the formation of quark-gluon plasma (QGP). The transition temperature is measured to be $T_c \sim 155$ MeV. Formation of the QGP and the consequent modification to the heavy-quark potential is expected to lead to different quarkonium states dissociating at different temperatures of the medium. It was found that the $\Upsilon(1S)$ persists well above $T_c$, while $\Upsilon(2S)$ dissociates at about $1.1T_c$ and $\Upsilon(3S)$ can not exist at temperatures above $T_c$.

The ATLAS experiment measured the $\Upsilon(nS)$ production cross-section in $pp$ and $Pb+Pb$ collisions at $\sqrt{s} = 5.02$ TeV per nucleon–nucleon pair [8]. The $Pb+Pb$ collisions studied in the

analysis were collected in the years 2015 and 2018 with integrated luminosities of $0.44\,\mathrm{nb}^{-1}$ and $1.38\,\mathrm{nb}^{-1}$, respectively. The integrated luminosity of the reference $pp$ sample collected in 2017 is $0.26\,\mathrm{fb}^{-1}$.

The analysis procedure relies on the categorization of the events in several centrality groups that define a degree of overlap between the two colliding Pb nuclei. The centrality estimate is based on the transverse energy measured in the forward calorimeter, $\sum E_{\mathrm{T}}^{FCal}$. Other important variables in the analysis are the mean number of participant nucleons $\langle N_{\mathrm{part}} \rangle$ and the mean nuclear overlap function $\langle T_{\mathrm{AA}} \rangle$ that are calculated from the Monte Carlo Glauber-based model.

The $\Upsilon(nS)$ states are reconstructed in the $\mu^+\mu^-$ decay channel. The reconstructed events are corrected by the weighting function that accounts for the acceptance corrections and various efficiencies. The overall resonance-dependent weight, $w_{\mathrm{total}}(\Upsilon(nS))$, is determined for each selected dimuon candidate as

$$w_{\mathrm{total}}(\Upsilon(nS)) = \frac{1}{\mathcal{A}(\Upsilon(nS)) \times \epsilon_{\mathrm{reco}}(\mu_1\mu_2) \times \epsilon_{\mathrm{trig}}(\mu_1\mu_2) \times \epsilon_{\mathrm{pvAsso}}(\mu_1\mu_2)},$$

where $\mathcal{A}(\Upsilon(nS))$ is the acceptance for $\Upsilon(nS) \rightarrow \mu^+\mu^-$ decay, $\epsilon_{\mathrm{reco}}$ is the muon reconstruction efficiency, $\epsilon_{\mathrm{trig}}$ is the trigger efficiency, and $\epsilon_{\mathrm{pvAsso}}$ is the efficiency related to the primary-vertex association.

The yields are determined via unbinned maximum-likelihood fits to the weighted di-muon invariant mass distributions, where each of the three $\Upsilon(nS)$ state signal shapes is described by a sum of Crystal Ball and Gaussian functions. Figure 5 shows an example of the fit to the dimuon mass plots for $pp$ (left) and 0–80% centrality $Pb+Pb$ (right) collisions for the inclusive $p_{\mathrm{T}}^{\mu\mu}$ and $|y^{\mu\mu}|$ selection.

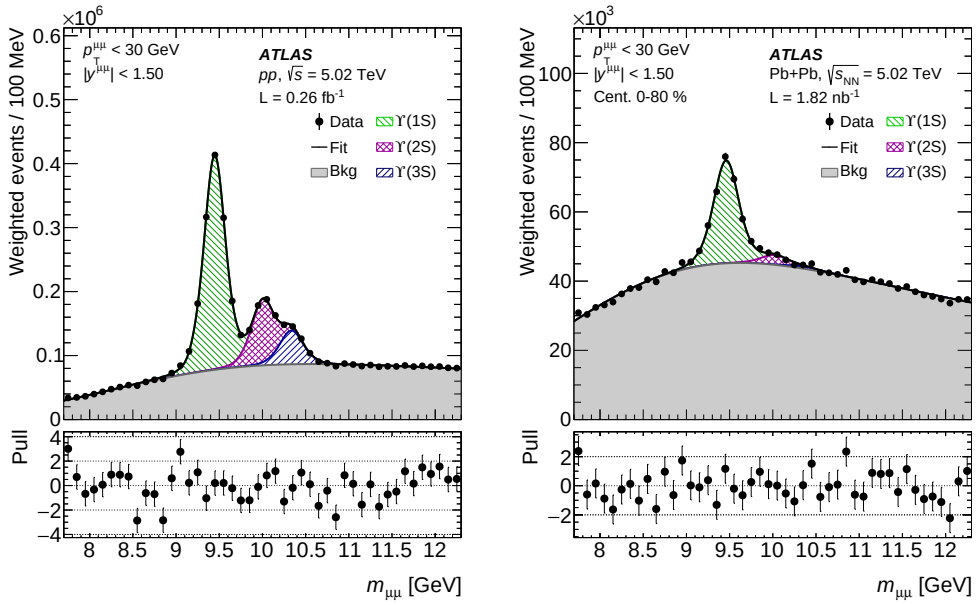


**Figure 5:** Dimuon invariant mass distributions with the fit results for $pp$ (left) and $Pb+Pb$ (right) collisions at 5.02 TeV. For this selection, $\chi^2$/NDF is 2.7 for $pp$ and 1.3 for $Pb+Pb$. Taken from [8].

The differential $\Upsilon(nS)$ production cross-sections in $pp$ collisions are measured according to the relation

$$\frac{d^2\sigma_{\Upsilon(nS)}}{dp_{\mathrm{T}}^{\mu\mu}dy^{\mu\mu}} \times \mathcal{B}(\Upsilon(nS) \to \mu^+\mu^-) = \frac{N^{\mathrm{corr}}_{\Upsilon(nS)}}{\Delta p_{\mathrm{T}}^{\mu\mu} \times \Delta y^{\mu\mu} \times \int \mathcal{L}dt},$$

where $\mathcal{B}(\Upsilon(nS) \to \mu^+\mu^-)$ is the dimuon decay branching fraction, $N^{\mathrm{corr}}_{\Upsilon(nS)}$ is the $\Upsilon(nS)$ yield corrected for acceptance and efficiencies, $\Delta p_{\mathrm{T}}^{\mu\mu}$ and $\Delta y^{\mu\mu}$ are the bin widths in $p_{\mathrm{T}}^{\mu\mu}$ and $y^{\mu\mu}$, and $\int \mathcal{L}dt$ is the integrated luminosity.

For the $Pb + Pb$ collisions we assume:

$$N_{AA} = \frac{N^{\mathrm{corr}}_{\Upsilon(nS)}}{\Delta p_{\mathrm{T}}^{\mu\mu} \times \Delta y^{\mu\mu} \times N\mathrm{evt}},$$

where $N_{\mathrm{evt}}$ is the total number of minimum-bias Pb+Pb collisions in each centrality class. The $\Upsilon(nS)$ differential cross-sections in both $pp$ and $Pb + Pb$ collisions are shown in Figure 6.

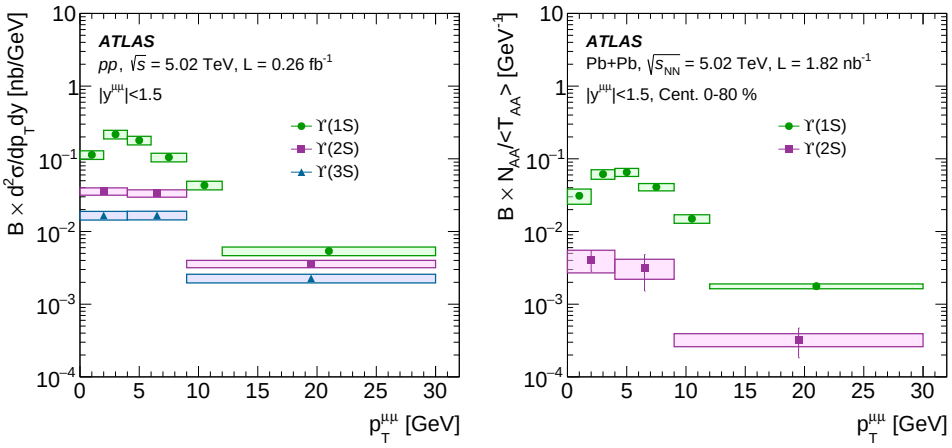


**Figure 6:** Production cross-sections of $\Upsilon(1S)$, $\Upsilon(2S)$, and $\Upsilon(3S)$ mesons as a function of $p_{\mathrm{T}}^{\mu\mu}$ in $pp$ collisions (left) and per-event yields in $Pb + Pb$ collisions (right) at 5.02 TeV. Taken from [8].

The modifications of bottomonium production yields in $Pb + Pb$ collisions relative to the $pp$ system are quantified by the nuclear modification factor $R_{AA}$, which can be defined for each centrality interval as

$$R_{AA} = \frac{N_{AA}}{\langle T_{AA} \rangle \times \sigma^{pp}},$$

where $N_{AA}$ is the observed per-event yield of bottomonium states in $Pb + Pb$ collisions, and $\sigma^{pp}$ is the bottomonium production cross-section in $pp$ collisions at the same collision energy.

Figure 7 shows the $R_{AA}$ values of $\Upsilon(nS)$ as a function of $\langle N_{\mathrm{part}} \rangle$ (top), dimuon $p_{\mathrm{T}}^{\mu\mu}$ (bottom left), and $|y^{\mu\mu}|$ (bottom right). The $R_{AA}$ value decreases with $\langle N_{\mathrm{part}} \rangle$ for all three states while for the $p_{\mathrm{T}}^{\mu\mu}$ and $|y^{\mu\mu}|$ no strong dependence is observed.

Upsilon suppression results were compared with the other LHC experiments that are operating at the same energy, and the measurements are consistent. The results are also compared with several theoretical calculations: by N. Brambilla et al. in Ref. [9], by X. Du et al. in Ref. [10] and by X. Yao et al. in Ref. [11]. All theoretical calculations considered in this paper describe the data well and incorporate deconfinement as a key ingredient in the suppression of the Upsilon yields.

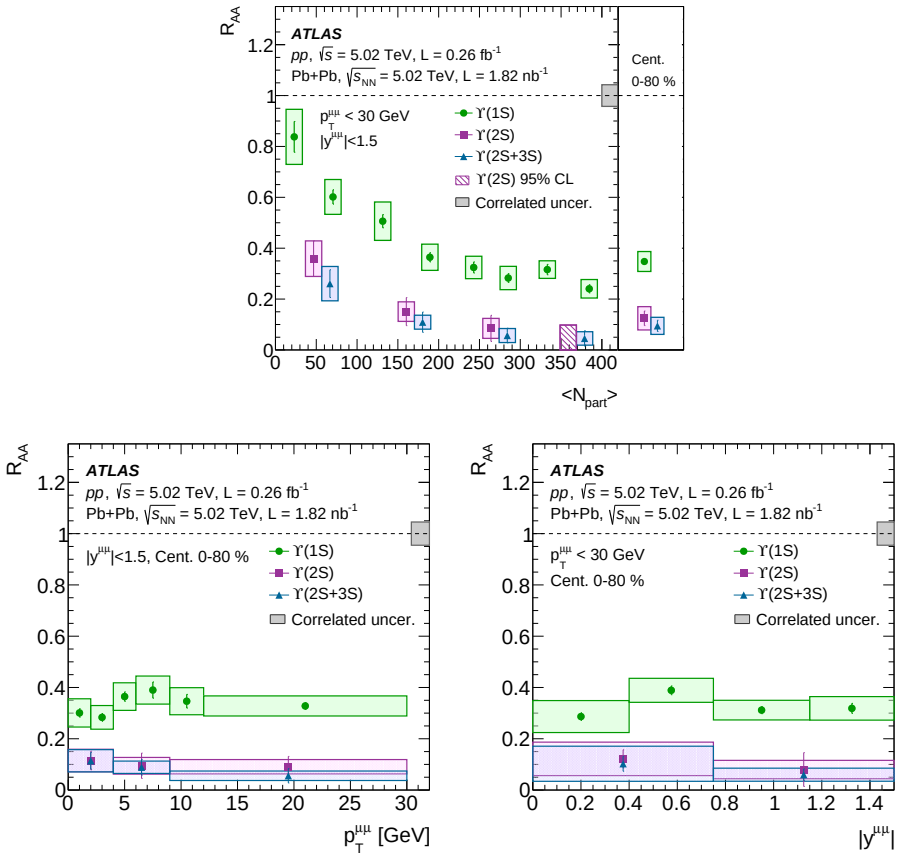


**Figure 7:** The nuclear modification factor $R_{AA}$ of $\Upsilon(1S)$, $\Upsilon(2S)$, and $\Upsilon(2S+3S)$ as a function of centrality (top), $p_{\mathrm{T}}^{\mu\mu}$ (bottom left), and $|y^{\mu\mu}|$ (bottom right) at 5.02 TeV. The error bars indicate the statistical uncertainties, and boxes represent the systematic uncertainties. The right panel of the top plot shows the $R_{AA}$ results integrated over centrality. Taken from [8].

## 3. Summary

The ATLAS experiment has a broad spectrum of heavy flavor measurements; the most recent results were presented. The measurement of $W$ production in association with charm decay $D^{(*)}$ shows a good agreement with predictions and provides useful constraints upon global PDF fits. The $\Upsilon(nS)$ production cross-section is also measured, and the nuclear modification factor is compared to various models. All results show good agreement with the previous LHC measurements as well as with the theoretical calculations.

## Acknowledgments

I acknowledge support from the National Science Foundation grant number 1906674.

## References


[1] L. Evans and P. Bryant, "LHC Machine," JINST **3** (2008), S08001

[2] G. Aad *et al.* [ATLAS], "The ATLAS Experiment at the CERN Large Hadron Collider," JINST **3** (2008), S08003

[3] G. Aad *et al.* [ATLAS], "Measurement of the production of a $W$ boson in association with a charmed hadron in $pp$ collisions at $\sqrt{s} = 13$ TeV with the ATLAS detector," Phys. Rev. D **108** (2023), 032012 [arXiv:2302.00336 [hep-ex]].

[4] S. Agostinelli *et al.* [GEANT4], "GEANT4–a simulation toolkit," Nucl. Instrum. Meth. A **506** (2003), 250-303

[5] [ATLAS], "Tools for estimating fake/non-prompt lepton backgrounds with the ATLAS detector at the LHC," [arXiv:2211.16178 [hep-ex]].

[6] M. Lisovyi, A. Verbytskyi and O. Zenaiev, "Combined analysis of charm-quark fragmentation-fraction measurements," Eur. Phys. J. C **76** (2016) no.7, 397 [arXiv:1509.01061 [hep-ex]].

[7] [ATLAS], "Reweighting heavy-flavor production fractions to reduce flavor modelling uncertainties for ATLAS," ATL-PHYS-PUB-2022-035.

[8] G. Aad *et al.* [ATLAS], "Production of $\Upsilon$(nS) mesons in Pb+Pb and pp collisions at 5.02 TeV," Phys. Rev. C **107** (2023) no.5, 054912 [arXiv:2205.03042 [nucl-ex]].

[9] N. Brambilla, M. Á. Escobedo, M. Strickland, A. Vairo, P. Vander Griend and J. H. Weber, "Bottomonium production in heavy-ion collisions using quantum trajectories: Differential observables and momentum anisotropy," Phys. Rev. D **104** (2021) no.9, 094049 [arXiv:2107.06222 [hep-ph]].

[10] X. Du, M. He and R. Rapp, "Color Screening and Regeneration of Bottomonia in High-Energy Heavy-Ion Collisions," Phys. Rev. C **96** (2017) no.5, 054901 [arXiv:1706.08670 [hep-ph]].

[11] X. Yao, W. Ke, Y. Xu, S. A. Bass and B. Müller, "Coupled Boltzmann Transport Equations of Heavy Quarks and Quarkonia in Quark-Gluon Plasma," JHEP **01** (2021), 046 [arXiv:2004.06746 [hep-ph]].


PoS(BEAUTY2023)042